Prog. Part. Nucl. Phys., Vol. 30, pp. 171–180, 1993.
Printed in Great Britain. All rights reserved.

0146–6410/93 $24.00

Target Fragmentation in Proton and Heavy-Ion Induced Reactions at High Energies

WA80 COLLABORATION: K. H. KAMPERT[4], R. ALBRECHT[1], T. C. AWES[5], P. BECKMANN[4,a], F. BERGER[4], M. BLOOMER[2], C. BLUME[4], D. BOCK[4], R. BOCK[1], G. CLAESSON[3], G. CLEWING[4], L. DRAGON[4,b], A. EKLUND[3], R. L. FERGUSON[5], A. FRANZ[5,a], S. GARPMAN[3], R. GLASOW[4], H. Å. GUSTAFSSON[3], H. H. GUTBROD[1], G. HÖLKER[4], J. IDH[3], P. JACOBS[2], B. W. KOLB[1], H. LÖHNER[4,c], I. LUND[1,c], F. E. OBENSHAIN[5], A. OSKARSSON[3], I. OTTERLUND[3], T. PEITZMANN[4], F. PLASIL[5], A. M. POSKANZER[2], M. PURSCHKE[4], H. G. RITTER[2], B. ROTERS[4], S. SAINI[5], R. SANTO[4], H. R. SCHMIDT[1], S. P. SØRENSEN[5,d], K. STEFFENS[4], P. STEINHAEUSER[4], E. STENLUND[3], D. STÜKEN[4] and G. R. YOUNG[5]

[1] *Gesellschaft für Schwerionenforschung, D-6100 Darmstadt, Germany*
[2] *Lawrence Berkeley Laboratory, Berkeley, CA 94720, U.S.A.*
[3] *University of Lund, S-22362 Lund, Sweden*
[4] *Universty of Münster, D-4400 Münster, Germany*
[5] *Oak Ridge National Laboratory, Oak Ridge, TN 37831, U.S.A.*
[a] *now at: CERN, Ch-1211 Geneva 23, Switzerland*
[b] *now at: Mercedes-Benz, D-7000 Stuttgart, Germany*
[c] *now at: KVI, University of Gronigen NL-9747 AA Gronigen, The Netherlands*
[d] *University of Tennessee, Knoxville, TN 37996, U.S.A.*

Abstract

Results on pseudorapidity distributions, azimuthal correlations, and on two particle interferometry for identified protons and pions measured in the target fragmentation region of high energy proton-nucleus and nucleus-nucleus collisions are presented. Full participation of the whole target nucleus is observed even for 200 GeV p + Au collisions. Incorporation of strong rescattering phenomena into string models, including pion absorption effects in excited target matter, provides a good description of most experimental data.

1 Introduction

The primary motivation for studying high-energy heavy-ion collisions at the CERN-SPS and Brookhaven-AGS accelerators is to investigate nuclear matter under conditions of extremely high densities and temperatures. Theoretical calculations predict that under such conditions hadronic matter might undergo a phase-transition to a new form of matter, the quark-gluon plasma (QGP), in which quarks and gluons are deconfined over an extended volume [1]. Unfortunately, a common characteristic of most of these signatures is the necessity to distinguish them from the large background created by ordinary hadronic processes. A thorough understanding of the reaction mechanism is, therefore, an important prerequisite in any search for the QGP.

Important information on the reaction mechanism can be gained from a comparison of nucleon-nucleus with nucleus-nucleus collisions. Deviations from a linear scaling are considered as an indicator for collective effects. Furthermore, studying hadron-nucleus interactions, offers the possibility to learn about the space-time development of high energy reactions. Such kind of investigation is not possible in elementary particle collisions (e.g. pp or $p\bar{p}$), because the target nucleons serve as detectors for reaction products at nuclear distances and time-scales not accessible with macroscopic detectors. Investigating the target fragmentation region in proton and light-ion induced reactions on different target nuclei thus offers an ideal tool to learn – in a macroscopic description – about the energy dissipation from the primary interaction zone to the so called "spectator matter" or to learn – in a microscopic description – about the interaction of produced particles with their high density nuclear environment as well as among produced particles themselves.

To address such questions, we present results from a comprehensive analysis of the target fragmentation region in p-, ^{16}O-, and ^{32}S-induced reactions at bombarding energies of 4.9, 60, and 200 AGeV across a large variety of target nuclei. We shall focus here on three different observables; pseudorapidity distributions and their target mass dependence (Sect. 3.1), azimuthal correlations between the forward and backward hemisphere with respect to the rest frame of the target system (Sect. 3.2), and two-particle interferometry (Sect. 3.3). All three observables are studied individually for pions and protons and are compared with results from the string models VENUS [2] and RQMD [3] which both incorporate rescattering phenomena of produced particles.

2 Experimental Setup and Data Reduction

The present data were measured by employing the Plastic-Ball spectrometer [4]. The Plastic-Ball is a modular, azimuthally symmetric array of 655 ΔE- E telescopes allowing particle identification and energy measurement for light baryons and positive pions. In its present configuration the detector covers the polar range of $30° \leq \vartheta_{\rm lab} \leq 160°$ $(1.3 \geq \eta \geq -1.7\,,\text{with}\ \eta = -\ln(\tan(\frac{\vartheta}{2}))\ )$.

The delayed signal of the sequential decay $\pi^+ \rightarrow \mu^+\nu_\mu \rightarrow e^+\nu_e\nu_\mu\bar{\nu}_\mu$ is used in addition to the ΔE-E measurement to make the identification of stopped positive pions unique and to prevent masking of pions by the more abundant baryons. Full identification is only achieved when the particles are stopped in the telescopes, limiting the accessible kinetic energy range to 20 – 120 MeV and 40 – 200 MeV for pions and protons, respectively. These cuts were applied to two-particle interferometry analyses. For the study of azimuthal correlations and for the target mass dependence of the yields, however, a wider energy range of 40 – 300 AMeV with limited identification is used for the baryons. To allow for a comparison with model predictions, all events from simulations were subjected to the same cuts in energy and coverage.

The angular region forward of the Plastic-Ball $(1.2 \leq \eta \leq 4.2)$ is complemented by two layers of Iarrocci-type streamer tube detectors with pad readout [5]. This detector does not provide particle identification but is used as charged particle tracking device and charged particle veto-detector for the photon spectrometer of the experiment [6].

3 Results

3.1 Charged Particle, Proton, and Pion Yields

Before restricting ourselves to examining the target region in more detail, it is instructive to study the variation of the global charged particle flow as a function of target mass. The almost 4π acceptance of the WA80 experiment for charged particle multiplicity measurements combined with the very high statistics is ideally suited for such kind of an analysis and allows a detection also of small variations. Figure 1 shows as an example the target mass dependence of the yield of charged particles as a function of pseudorapidity for central collisions of 200 AGeV S + Au, Ag, and Cu [7]. The yield is assumed to follow a power-law behavior on the target mass number A_t, i.e. $dN_{ch}/d\eta \propto A_t^\alpha$, where α is determined as a function of pseudorapidity. The value of $\alpha \simeq 1$ in the target fragmentation region

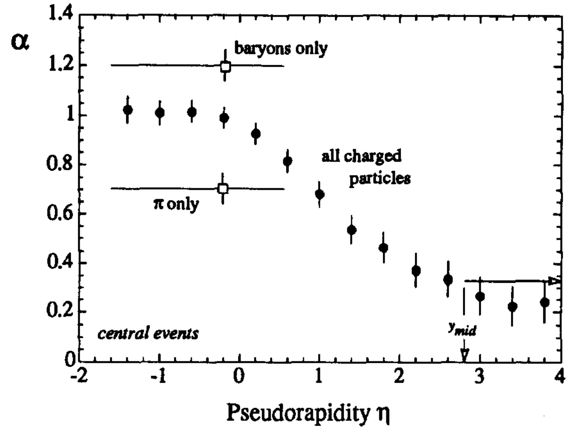

Fig. 1: Target mass dependence of the charged particle yield, expressed as $dN/d\eta \propto A_t^{\alpha(\eta)}$, as a function of pseudorapidity for 200 AGeV S + Au, Ag, and Cu reactions. The two open symbols represent the values extracted from the transverse energy in O+Nucleus data [8] in the indicated pseudorapidity range for baryons and pions, respectively.

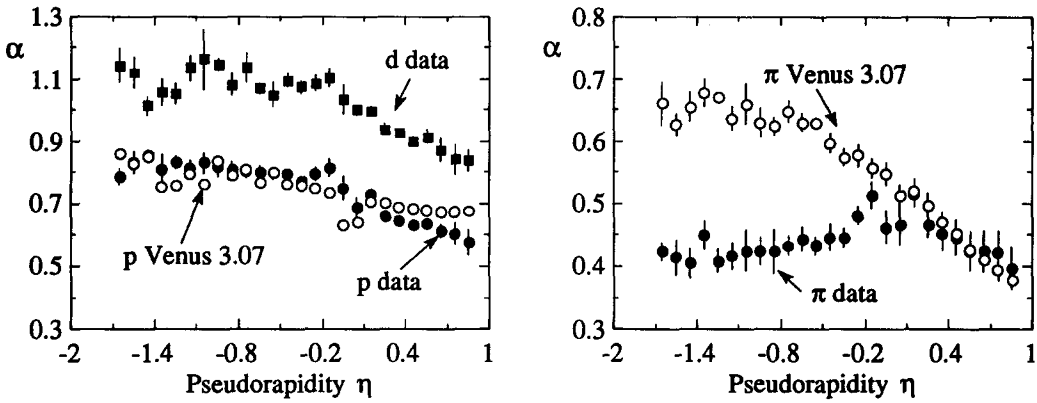

Fig. 2: Target mass dependence of the yield of deuterons, protons, and pions as a function of pseudorapidity for 200 AGeV p + Au, Ag, Cu, C. The target dependence is parameterized as $dN/d\eta \propto A^{\alpha(\eta)}$. The open symbols show the results of VENUS 3.07 simulations.

($\eta \leq 0$) indicates a strong excitation of the target matter, i.e. the whole target nucleus participates in the reaction. At mid-rapidity ($\eta \approx 2.8$) a value of $\alpha \simeq 1/3$ is found (see arrows in Fig. 1) which happens just to be the value expected by a simple geometrical fireball picture in this region for asymmetric systems. A related analysis has been performed in Ref. [8], where the transverse energy of baryons and pions observed in the target region ($-1.7 \leq \eta \leq 0.6$) has been studied in oxygen induced data by making use of the particle identification capability of the Plastic-Ball. The results are included in Fig. 1 and yield α-values of approximately 0.7 for pions and a value even larger than one for baryons [8]. Using a more realistic, but model dependent parametrisation, namely $E_\perp \propto (A_t - A_{\mathrm{participants}})^\alpha$ = (number of target participants)$^\alpha$, one obtains $\alpha = 0.62$ and 1.04 for pions and baryons, respectively. Furthermore, the transverse energy observed at backward rapidities amounts to roughly 20 % of the $E_\perp$ measured around mid-rapidity ($2.4 \leq \eta \leq 5.5$). The results on the yields and transverse energies thus demonstrate a strong excitation and full participation of the target nucleus in Oxygen and Sulfur-induced reactions at SPS energies.

Figure 2 shows the results of a similar analysis for proton induced reactions at 200 GeV. Again, the target mass dependence is displayed in terms of the exponent α, shown now differentially for deuterons, protons, and pions. Similarly to above, a stronger and almost linear dependence of the baryon multiplicity on the target mass is deduced, while the pion yield grows only like $A_t^{0.4}$ at backward rapidities. Quantitatively, we may conclude that the whole target nucleus is involved in the baryon emission, but that the pion yield is largely determined by the volume of the primary interaction zone. The η-dependence of the target mass dependence of the proton yield is well reproduced by the event generator VENUS 3.07 [2]. This model incorporates rescattering effects of secondaries among themselves and with other particles, which was found to be a major source of target protons [2]. In fact, the model describes not only the variation of the proton yield with target mass, but also the absolute value of the pseudorapidity distributions rather well [9]. On the other hand, the increase of the pion yield with target mass is overestimated by about 50 % at very backward rapidities and a good description of their pseudorapidity distributions in the target region is only found in case of light targets [9]. It should be pointed out, that the same model with the rescattering mechanism switched off clearly fails in describing the yields of both baryons and pions.

3.2 Azimuthal Correlations of Protons and Pions

Additional information than from the proton and pion yields alone can be gained from studying collective structures in the particle emission. A possible azimuthal correlation between protons or between pions in target rapidity region is investigated by constructing a correlation function $C(\Delta\varphi) := dN/d(\Delta\varphi)$ as follows:

$$\Delta\varphi = \arccos\left(\frac{\vec{Q}_{\text{back}} \cdot \vec{Q}_{\text{forw}}}{|\vec{Q}_{\text{back}}| \cdot |\vec{Q}_{\text{forw}}|}\right) \quad ; \quad \vec{Q}_{\text{back}} := \sum_{y \le y_0} \vec{p}_\perp^{\,i} \quad \text{and} \quad \vec{Q}_{\text{forw}} := \sum_{y > y_0} \vec{p}_\perp^{\,i}$$

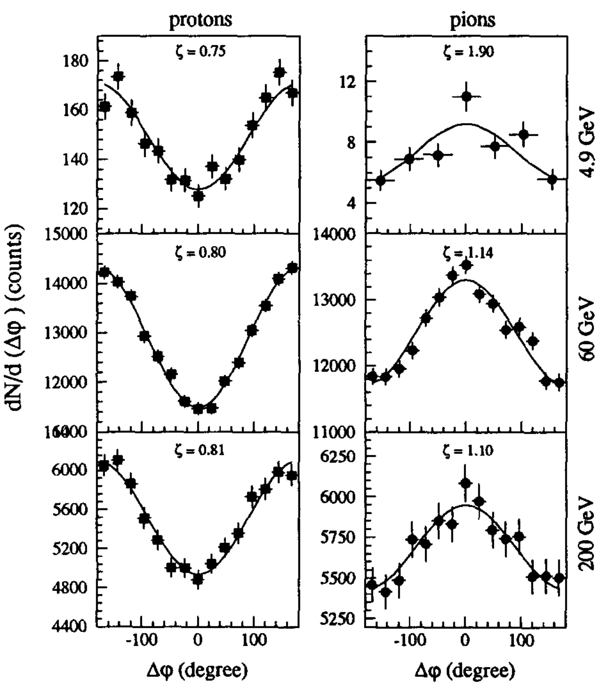

Fig. 3: Azimuthal correlation, $C(\Delta\varphi)$, between particles emitted forward and backward with respect the rest frame of the target nucleus (see text for definition). The left panel shows the correlations for protons and the right panel for pions, emitted from p + Au collisions at 4.9 (top), 60 (center) and 200 GeV (bottom) incident energy.

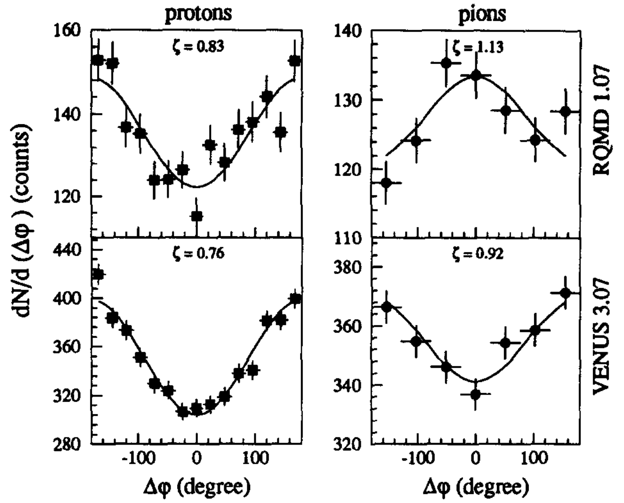

Fig. 4: Azimuthal correlation function as in Fig. 3, but for simulated p + Au collisions at 200 GeV. The top and bottom plots are from VENUS and RQMD simulations, respectively.

The value of y_0 is chosen as 0.2, guided by the idea of a target fireball moving with a rapidity y_0 and is also supported by the fact that the rapidity distributions of protons peak at this value. A correlation function defined in such a way inspects the difference in azimuth between the particles emitted forward and backward relative the rest frame of the target nucleus. For pions, where the kinetic energy is mostly not measured, $\vec{p}_\perp$ is replaced by $\vec{r}_\perp$, the transverse coordinate. Experimental results for protons and pions are shown in Fig. 3 for p + Au reactions at 4.9, 60, and 200 GeV incident energy. A remarkable difference is found between protons and pions: the proton correlation functions show a depletion while the pions show an enhancement at $\Delta\varphi = 0°$. Protons are thus emitted preferentially *back-to-back* and pions *side-by-side* in azimuth. To quantify the strength of the correlation, the data were fitted by $C(\Delta\varphi) \propto 1 + \xi\cos(\Delta\varphi)$ so that

$$\zeta := \frac{C(0°)}{C(180°)} = \frac{1+\xi}{1-\xi}$$

provides a measure of the correlation strength. The strongest correlation is found for 4.9 GeV p + Au reactions where almost twice as many pions are emitted into one direction than diametrical to that. At this bombarding energy, however, only positive pions with energies below 120 MeV were taken into account. Before discussing these interesting observations, we confront the VENUS and RQMD models to the experimental data in Fig. 4. As can be seen from that figure, both models are able to describe the azimuthal correlations of protons fairly well. In case of pions, however, only RQMD seems to reproduce the data, VENUS on the other hand predicts a behavior opposite to the one observed both experimentally and in RQMD.

We conjecture that the reason for the observed differences between proton- and pion-yields, as discussed in the previous section, and their azimuthal correlations is due to pion absorption in the excited target matter. Since heavy-ion reactions are dominated by soft collisions, there is a large cross section for Δ-formation and higher resonances. Once the Δ's are produced, they will again interact with surrounding target nucleons or with other Δ's;

$$\pi + N \rightarrow \Delta \quad \text{and} \quad \left\{ \begin{array}{l} \Delta + N \rightarrow N + N \\ \Delta + \Delta \rightarrow N + N \end{array} \right.$$

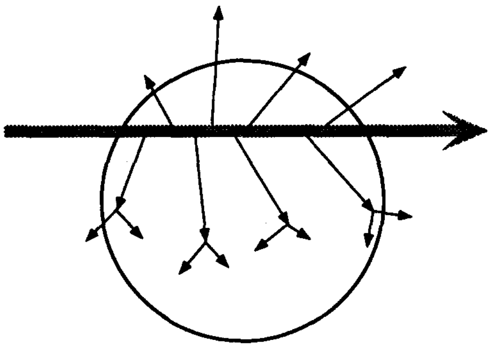

Fig. 5: Schematic view of a non-central pA collision. Pions created along the path of the incident projectile are partially absorbed in the target matter.

Possible re-emission of pions by Δ-decays occurs basically isotropic and those pions subsequently may again be absorbed into resonance states, as listed above. Such processes will thus effectively lead to a directional absorption of pions and thereby to a heating up of the target nucleus that subsequently decays mainly by nucleon emission. Consequently, the target dependence of the proton yield will grow proportional to the number of target 'spectator' nucleons, while pion yield remains essentially the one generated by primary collisions of the projectile with the target nucleons, resulting in a growth like $dN_\pi/d\eta \propto A_t^{1/3}$.

The interpretation in terms of (directed) pion absorption is independently supported by the experimentally observed azimuthal correlations. While the back-to-back emission of protons can be understood as resulting from transverse momentum conservation, the pion correlations can be explained based on the geometrical picture that pions created in a $b \neq 0$ collision experience a more probable absorption into resonance states on the far side of the impact as depicted schematically in Fig. 5. A very similar effect of pion absorption has also been observed by the Diogene Collaboration in Ne + Pb collisions at 800 AMeV [10].

Interestingly, the RQMD model reproduces the observed pion correlation. This might be due to the fact that this model employs energy dependent experimentally measured cross sections for πN reactions that are in the low energy region dominated by Δ-resonance excitation. VENUS on the other hand, assumes a unique, energy independent minimal distance approach below which secondary interactions occur. The thereby essentially ignored pion absorption by resonance formation also seems to explain, why VENUS overestimates the growth of the pion yield with increasing target mass at very backward rapidities (see Fig. 2).

3.3 Two-Proton and Two-Pion Correlations

Two-particle interferometry recently has attracted much attention in nuclear reactions because it carries information about the space-time characteristics of the particle emitting source. In view of the peculiar differences found in the previous two sections between proton and pion emission, it is instructive to investigate proton-proton and pion-pion correlations in the same region of phase space and to compare their results. However, the mechanism causing the correlation at small relative momenta of protons and pions, respectively, is quite different and should be kept in mind in such a direct comparison. The emphasis will thus be more on the *variation* of the correlation with target mass, rather than to directly oppose their absolute values.

The shape of the two-proton correlation function reflects an interplay of the short range nuclear interaction, the Pauli exclusion principle, and the long range mutual Coulomb repulsion of the two protons [11]. The strong S-wave attraction leads to a pronounced maximum in the two-proton

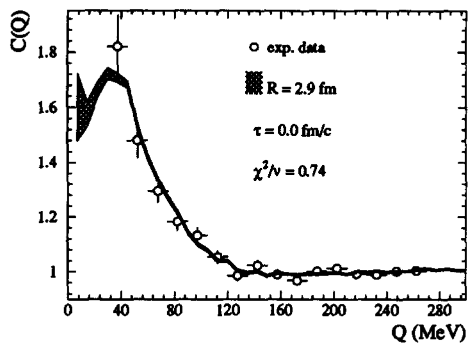

Fig. 6: Two-proton correlation function in dependence of $Q = |\vec{p}_1 - \vec{p}_2|$ for 200 GeV p + Cu collisions. The hatched band represents the result of a simulation as described in the text.

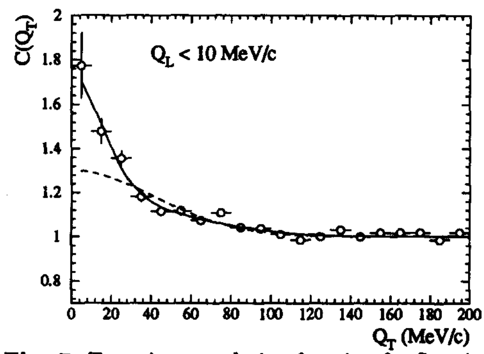

Fig. 7: Two-pion correlation function for S + Au collisions at 200 AGeV. The solid line is the result of a two-component, and the dashed line the result of a single-component Gaussian fit to the data.

correlation function at relative momentum $Q = |\vec{p}_1 - \vec{p}_2| \simeq 40$ MeV/c when the average distance upon emission is of the order of 10 fm or less [12]. The long range Coulomb interaction and the Pauli exclusion principle lead to to a minimum at $Q = 0$. Examples of two-proton correlation studies performed at beam energies of approximately 50 AMeV to 14.6 AGeV can be found in Refs. [12,13,14]. Since there is no simple analytical expression for the correlation function possible, a simulation is used to calculate the two-particle amplitude based on the measured single-particle distributions and including the effects mentioned above [15]. A spherical source with a life time of $\tau = 0$ fm/c is assumed and the detector resolution is taken into account in the simulation. The best fit to the data is determined by repeating the simulation for different radii and calculating the χ^2/ν from a comparison with the data. An example of a two-proton correlation function together with the result of the simulation is given in Fig. 6.

Two-pion interferometry – known as Bose-Einstein correlation – is a widespread tool to study the space-time properties of the particle emitting source in high energy collisions [16]. A simple theoretical picture of multiparticle production yields $C(p_1^\mu, p_2^\mu) = 1 + \lambda|\tilde{\rho}(p_1^\mu - p_2^\mu)|^2$ for the correlation function, where $\tilde{\rho}$ is the Fourier transform of the distributions of emitters and λ is a parameter describing the experimentally observed correlation strength. The width of the correlation function thus is inversely proportional to the size of the source. An example of a $\pi^+\pi^+$ correlation function is shown in Fig. 7 for 200 AGeV S + Au reactions. Two different fits are applied to the data, a standard single Gaussian and a two-component Gaussian to account for the strong enhancement of correlated pions at small relative momenta,

$$C(Q_T, Q_L) = 1 + \lambda \cdot \exp\left(-\frac{Q_T^2 R_T^2}{2} - \frac{Q_L^2 R_L^2}{2}\right) \tag{1}$$

$$C(Q_T, Q_L) = 1 + \left[\lambda_1 \cdot \exp\left(\frac{-Q_T^2 R_{T1}^2 - Q_L^2 R_{L1}^2}{4}\right) + \lambda_2 \cdot \exp\left(\frac{-Q_T^2 R_{T2}^2 - Q_L^2 R_{L2}^2}{4}\right)\right]^2 \tag{2}$$

where Q_T and Q_L is the transverse and longitudinal momentum difference, respectively. A Gamow correction is applied to correct for Coulomb repulsion. Furthermore, a two-pion pair efficiency correction was deduced from the data to correct for pair losses at small relative opening angles. As can be seen from Fig. 7, the assumption of a single Gaussian for the pion emitter (dashed line) provides a rather poor description for the data. However, for simplicity, we will first discuss the results of the one-component Gaussian fits and return to the two-component fits later.

The results of the proton-proton and pion-pion correlations are compiled in Fig. 8 for p, O, and S-induced reactions at 200 AGeV. A distinct variation of the source parameters as a function of target

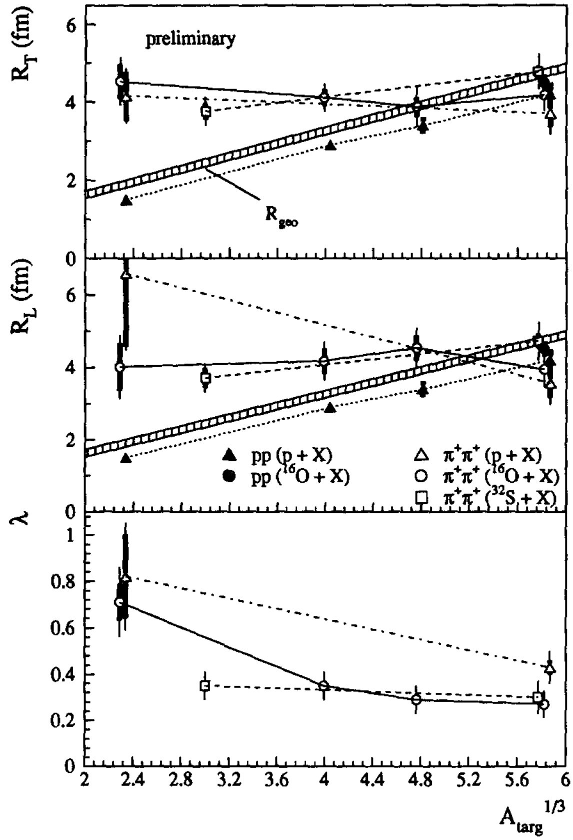

Fig. 8: Two-proton and two-pion correlation parameters as a function of target mass for 200 AGeV (p, O, S) + (C, Al, Cu, Ag, Au). The hatched band represents the equivalent Gaussian radii of the target nuclei.

mass is observed for the pp-correlations; their radius parameter increases like $A_t^{1/3}$ and happens to be very close to the spatial extent of the target nucleus. No significant variation, on the other hand, is observed for the target mass dependence of the transverse and longitudinal radii as extracted from $\pi^+\pi^+$ correlations. Both radii are found to be of the order of 4 fm/c for all systems. In case of the C-target, where the fits describe the experimental correlation function rather well [17], the extracted radii are larger than the sizes of the involved nuclei which might indicate transverse expansion prior to freeze-out. Going to heavier targets we observe, however, decreasing values for the λ-parameters. The physical meaning of this quantity is not fully understood and still subject of discussion [18], but its variation indicates that only a smaller fraction of correlated pion-pairs is perceptible to this correlation analysis in case of heavy targets. In fact, inspecting the correlation functions in more detail, traces this variation back to an increasing abundance of correlated pions at small relative momenta that cannot be fitted by a single Gaussian distribution (see Fig. 7).

To help unraveling the reasons for the variations of the pion correlation function, we introduce a second component to the fit function (see eq. 2). Only this provides a good description over the whole range of data and allows us to study the variation of the correlation function on a more reliable basis. Preliminary results of such an analysis are displayed in Fig. 9 for (p, O, S) + Au reactions at 200 AGeV. Instead of plotting the extracted radii of impact parameter averaged data in dependence of the target mass, the data are now centrality selected and presented in dependence of the average number of protons observed in the Plastic-Ball. In such kind of plot, all data follow

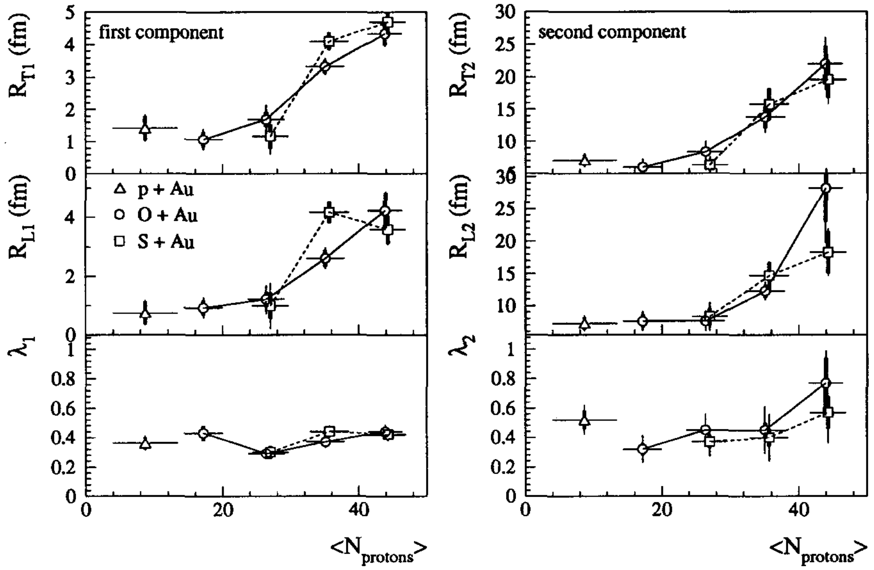

Fig. 9: Preliminary results of a two-component fit to the $\pi^+\pi^+$ correlation function. Shown are the extracted transverse- and longitudinal radii and λ-values for 200 AGeV (p, O, S) + Au as a function of the number of protons observed in the target fragmentation region. The thick vertical lines represent systematic, and thin lines statistical errors.

now the same trend of strongly increasing radii with increasing proton multiplicity. Furthermore, the proton multiplicity seems to provide a common scaling variable for all systems. While the radius parameter of the first component increases from approximately 1 fm to 4-5 fm, the parameter of the second component, describing the correlation at small values of Q, grows to values as large as about 15 fm. The λ-parameter is approximately 0.5 for both components and shows only little variation with proton multiplicity.

4 Summary and Discussion

We have presented comprehensive results on identified protons and pions measured in the target fragmentation region of proton-nucleus and nucleus-nucleus reactions for various targets and three bombarding energies (4.9, 60, and 200 AGeV). The experimental pseudorapidity distributions are generally well described by VENUS calculations. Exceptions are the yields at very backward pseudorapidities, where the proton and pion yields are under- and overestimated, respectively, by VENUS. The proton yield and their integrated transverse energy is proportional to the number of target spectators and its growth is well reproduced by VENUS for all η-windows. The increase of the pion yield with target mass, however, is overestimated by VENUS.

Distinctive differences in the proton and pion emission are also found in their azimuthal correlations relative to the center of mass system of the target fireball. Protons appear to be emitted azimuthally back-to-back, while pions are observed side-by-side. The former effect can be understood as a consequence of (local) transverse momentum conservation, and the latter effect suggests strong pion absorption effects occurring – mainly by Δ-excitations – in the excited target matter. RQMD includes all known low-lying resonance states and is, contrary to VENUS, able to to describe the experimental data both qualitatively and quantitatively.

Two-particle correlations, finally, show an increase of the proton emitting source proportional to the radius of the target nucleus, and a rather complicated behavior for $\pi^+\pi^+$ correlations, mainly established by an increasing fraction of pion-pairs found at very small values of Q for heavy targets. These data could successfully be described by a two-component fit and increasing $\pi^+\pi^+$ radius parameters are observed with increasing proton multiplicity independent of the reaction system.

Summarizing all these independent results of the target fragmentation region, we seem to arrive at a rather consistent picture.

The proton multiplicity is proportional to the number of target 'spectators', there is no preferred direction in their emission, and the radius parameter of the proton emitter grows proportional to the radius of the target nucleus. This leads to the conclusion that the whole target nucleus participates in the reaction not only in Oxygen- and Sulfur-, but also in proton induced reactions up to 200 AGeV.

A more complex behavior is found for the pion emission. All experimental findings suggest that pion absorption effects play an important rôle for an understanding of the target excitation and fragmentation; (i) the yield grows approximately like $A_t^{0.4}$ and $A_t^{0.6}$ for proton- and O-induced reactions, respectively, which is weaker than predicted by a model without absorption, (ii) the emission pattern exhibits a preferred direction to one side, which is only reproduced by a model including π-absorption, and (iii) the correlation functions show an increasing fraction of correlated pion-pairs at small relative momenta with increasing target mass. In previous publications [17,19] we argued that this enhanced correlation, which can be accounted for by a large radius parameter of a second component, could be taken as a hint to rescattering phenomena. Interestingly, Bauer reported on this conference on a very similar structure observed in BUU-based calculations, where inclusion of pion absorption effects leads to an enhancement in the correlation function at small values of Q [20]. We expect that a quantitative comparison done directly via the correlation functions, rather than indirectly via the extracted fit parameters, will help to shed more light onto the physics behind two pion correlations.

Acknowledgment

It is a pleasure to warmly thank the organizers for inviting KHK to attend the interesting and successful school on fascinating aspects of nuclear physics at intermediate and high energies. Partial support by the West German BMFT, DFG, GSI, the United States DOE, the Swedish NFR, the Italian CNdR, and the CERN PPE Division is gratefully acknowledged. In preparing this talk I have significantly profited from active support by my colleagues C. Blume, T. Peitzmann, and H.R. Schmidt.

References

[1] See most recent Quark Matter proceedings; Nucl. Phys. **A544** (1992), Nucl. Phys. **A525** (1991), Nucl. Phys. **A498** (1989), Z. Phys. **C38** (1988)
[2] K. Werner, P. Koch, Phys. Lett. **B242** (1990) 251
[3] H. Sorge, *et al.*, Z. Phys. **C47** (1990) 629
[4] A. Baden, *et al.*, Nucl. Inst. Meth. **A203** (1982) 189
[5] R. Albrecht, *et al.*, Nucl. Inst. Meth. **A276** (1989) 131
[6] See e.g.: R. Santo, *et al.*, proceedings to this conference
[7] R. Albrecht, *et al.*, Z. Phys. **C55** (1992) 539
[8] R. Albrecht, *et al.*, WA80 Collaboration, Z. Phys. **C45** (1990) 529
[9] R. Albrecht, *et al.*, WA80 Collaboration, Target Fragmentation Paper, in preparation
[10] J. Gosset, *et al.*, Diogene Collaboration, Phys. Rev. Lett. **62** (1989) 1251
[11] S.E. Koonin, Phys. Lett. **70B** (1977) 43
[12] D.H. Boal, C.K. Gelbke, and B.K. Jennings, Rev. Mod. Phys. **62** (1990) 553
[13] H.Å. Gustafsson, *et al.*, Plastic-Ball Collaboration, Phys. Rev. Lett. **53** (1984) 544
[14] B. Zajc, *et al.*, E802 and E859 Collaboration, Nucl. Phys. **A544** (1992) 237c
[15] We have benefitted enormously from a computer code provided by S. Pratt
[16] G.I. Kopylov, M.I. Podgoretskii, Sov. J. Nucl. Phys. **15** (1972) 219; **18** (1974) 336; M. Gyulassy, S.K. Kauffmann, L.W. Wilsonn, Phys. Rev. **C20** (1979) 2267, R. Stock, Ann. der Physik **48** (1991) 195
[17] R. Albrecht, *et al.*, WA80 Collaboration, Z. Phys. **C53** (1992) 225
[18] T. Peitzmann, Z. Phys. **C55** (1992) 485
[19] K.H. Kampert, *et al.*, WA80 Collaboration, Nucl. Phys. **A544** (1992) 183c
[20] W. Bauer, private communication and proceedings to this conference